Canonical Profiles Transport Model for H-mode Shots in Tokamaks

A.Yu. Dnestrovskij 1), Yu.N. Dnestrovskij 1), S.V. Cherkasov 1), A.V. Danilov 1), S.N. Gerasimov 2), T.C. Hender 2), S.E. Lysenko 1), I. Voitsekhovitch 2), C.M. Roach 2), M.J. Walsh 2) and JET EFDA* and MAST contributors

1) Russian Research Centre "Kurchatov Institute", Institute of Nuclear Fusion, Moscow, RF
2) EURATOM/UKAEA Fusion Association, Culham Science Centre, Abingdon, Oxon, OX14 3DB, UK

*See the Appendix of F.Romanelli et al., paper OV/1-2, this conference.

e-mail contact of main author: dnyn@nfi.kiae.ru

Abstract. The Canonical Profiles Transport Model (CPTM), which includes both the heat and particle transport equations, is used to simulate core and pedestal plasma for JET, and MAST H-mode shots. Simulations show reasonable agreement with experiment for both ELMy and ELM-free shots. RMS deviations of calculated results from the experimental ones are on the level 10-12% in main. The calculated ion and electron temperatures are very insensitive to the change of the deposited power profiles. The calculated pedestal temperature rapidly increases with plasma current; density profile peaking increases at low collisionalities.

1. Introduction

It is well known that the temperature and pressure profiles in tokamaks are self-consistent [1-4]. The self-consistency of temperature profiles guided the construction of an equation for the heat conductivity in terms of so called "critical temperature gradients" [5-7]. In our previous works this critical gradient was expressed through the gradient of the canonical temperature profile [8, 9]. The self-consistency of pressure profiles allowed us to construct the particle flux similarly to the heat flux [3, 4]. In this report the proposed Canonical Profiles Transport Model (CPTM), which includes both the heat and particle transport equations, is used to simulate sets of JET, and MAST H-mode shots. We use the non-linear version of the CPTM, which simulates the evolution of profiles of plasma temperatures and density including their pedestals. The non-linear version is based on the so-called "forgetting effect", which leads to bifurcation in the transport equations. The bifurcation takes place, when the relative deviation of the calculated pressure gradient from the canonical one, in the vicinity of the plasma edge, exceeds some critical value. The boundary conditions for the electron and ion temperatures and for plasma density are set at the separatrix, and therefore the region of the External Transport Barrier (ETB) is included in the model.

2. Basic equations and statement of problem

The heat and particle fluxes, q_α (α = e, i), Γ, are described by the following expressions:

$$q_\alpha = -n\chi_\alpha^{PC} T_\alpha \left(T_\alpha'/T_\alpha - T_c'/T_c\right) H\left(-\left[T_\alpha'/T_\alpha - T_c'/T_c\right]\right) F_\alpha - n\chi_\alpha^{0} T_\alpha' + 3/2\, \Gamma T_\alpha \qquad (1)$$

$$\Gamma = -D\, n \left(p_e'/p_e - p_c'/p_c\right) F_e F_i - D^0 n' + \Gamma^{neo}, \qquad (2)$$

where T_α and n are the temperatures and density to be determined, T_c and p_c are the canonical profiles of temperature and pressure, χ_α^{PC} and D are stiffness coefficients, $\Gamma^{neo} = n\, v^{neo}$, $H(x)$ is the Heaviside function, ρ is a radial coordinate ($0 < \rho < \rho_{max}$), $'$ denotes the radial derivative. The values of χ_α^{PC} were found by the comparison of calculations with experiment [9, 10]:

$$\chi_\alpha^{PC} = C_{T\alpha} (1/M) (a/R)^{0.75} q(\rho = \rho_{max}/2) q_{cyl} \left(T_e(\rho = \rho_{max}/4)\right)^{1/2} (3/R)^{1/4} (1/B_0)\ \bar{n}/n \qquad (3)$$

The values of χ_α^0 are much smaller than χ_α^{PC}, but play an essential role inside the transport barriers. We set also [3, 4] $D = C_n \chi_e^{PC}$, $C_n = 0.08$. This value of C_n leads to a reasonable range of the required cold neutrals influx $q_N = (2 – 20)\times10^{21}$ s^{-1}, depending on plasma density and deposited power. We propose also that $p_c \sim i_c$ and $T_c'/T_c = 2/3\ p_c'/p_c$, where p_c and i_c are the dimensionless canonical profiles for pressure and current density. The derivation of the canonical profiles $\mu_c=1/q_c$ and i_c was discussed in [4,8].

In expressions (1)-(2) $F_\alpha = \exp(-z_{p\alpha}^2/2z_0^2)$ is a "forgetting factor", where $z_{p\alpha}= -(a\ \rho_{max}/\rho)(p_\alpha'/p_\alpha - p_c'/p_c)$ is a dimensionless "distance" between the electron or ion pressure profiles and the canonical pressure profile. We suppose that a transport barrier occurs, when the distance $z_{p\alpha}$ exceeds the second critical gradient z_0: $|z_{p\alpha}|>z_0$. To describe the H-mode, it is sufficient to set $z_0 = 8$ [9, 10]. Note that in the transport barrier (the forgetting region) $F_k << 1$ and the first terms in fluxes (1, 2) will be small, but outside this region $F_k \approx 1$.
To estimate the quality of simulation, we introduce the RMS deviations for temperatures:

$$d_2T=\{(1/N)\sum_k^N[\frac{T_k^{calc}-T_k^{exp}}{T_k^{exp}}]^2\}^{1/2} \qquad (4)$$

and similar values for density. The summation is produced over points placed in the region $0<\rho<0.8\rho_{max}$, as the experimental data are less reliable near the plasma edge. As boundary conditions for temperatures and density we set $T_e(a) = T_i(a) = 0.05$ keV, $n(a) \sim \bar{n}/10$.

3. Simulation of JET ELMy H-mode shots

The simulation is carried out for two groups of JET shots. The first group contains shots with a broad range of plasma current, and was used in [11, 12]. The second group includes shots with small and large values of collisionality parameter ν_{eff}, which is proportional to n/T_e^2. Figure 1 shows the distribution of chosen shots in the (n, P_{tot}) plane. We use in this section the experimental data as analysed using the TRANSP code.

To construct the transport barrier model, we have to specify the coefficients χ_i^0, χ_e^0 and D^0, which define the behaviour of plasma parameters inside the external transport barrier (ETB). Model parameters were optimised for the chosen sets of shots to give:

$$\chi_i^0 = 0.23\ P_{tot}/(\langle n\rangle I_p),\ \ \chi_e^0 = \chi_i^0\ \{4.5\ (T_e)^{1/2}/R\}\ (m^2/s) \qquad (5)$$

$$D^0 = 0.4\ (T_e(0))^{1/2}/(\langle n\rangle R)\ (m^2/s) \qquad (6)$$

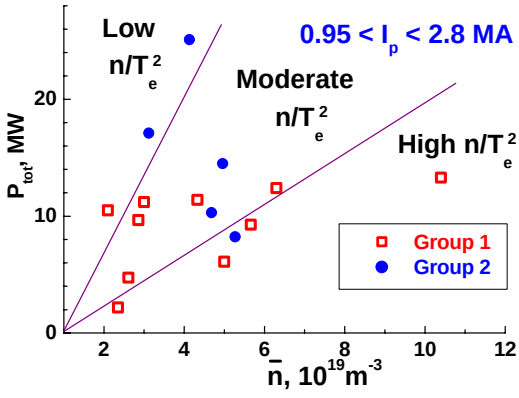

FIG. 1. Main parameters of chosen JET H-mode shots.

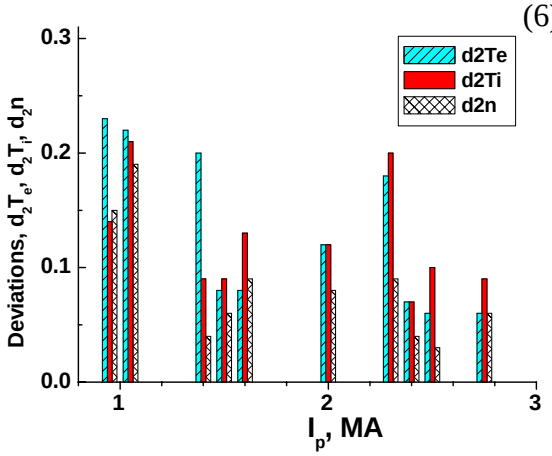

FIG. 2. RMS deviations for the first group of shots.

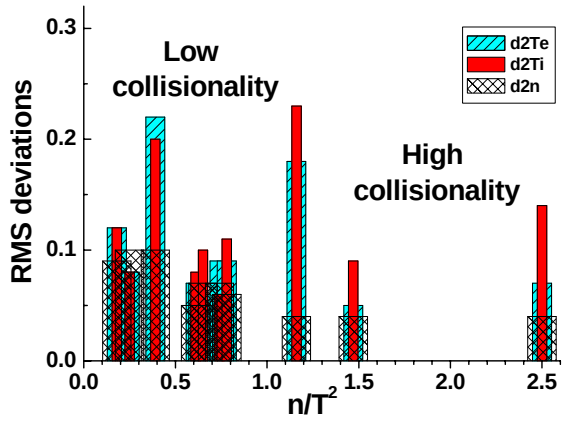

FIG. 3. RMS deviations for 10 JET shots with current I_p > 1.5 MA vs collisionality.

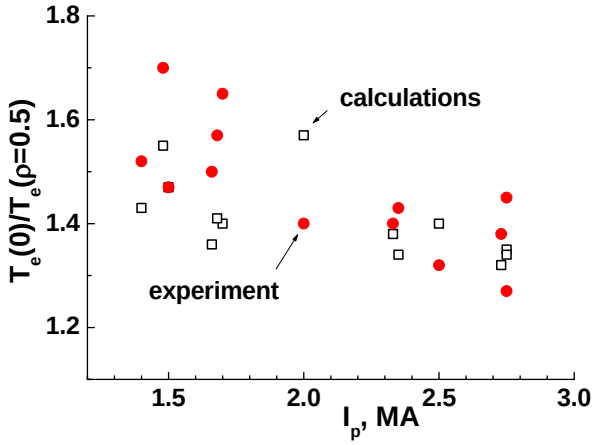

FIG. 4. Peaking of experimental (red circles) and calculated (black squares) electron temperature profiles vs plasma current.

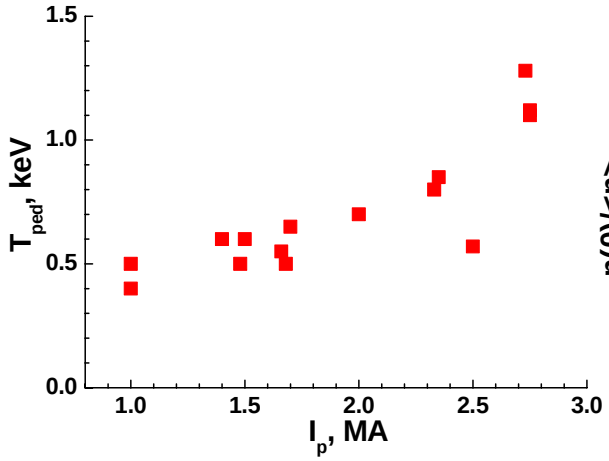

FIG. 5. Calculated temperature pedestal vs current.

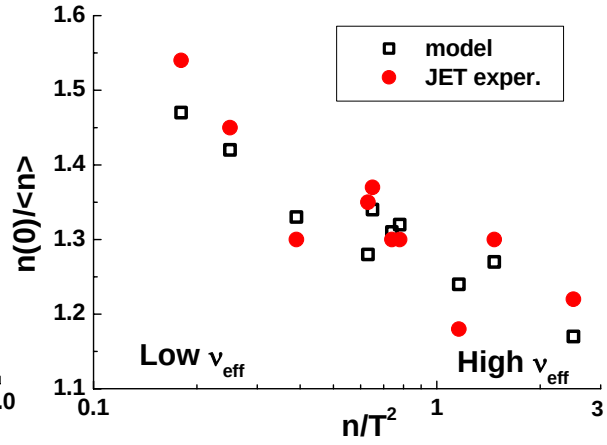

FIG. 6. Experimental and calculated density peaking for shots with I_p>1.5 MA.

Here n, I_p, P_{tot}, R and T_e are in 10^{19} m^{-3}, MA, MW, m, keV correspondingly, and <…> denotes volume-averaging. The quality of the simulation is displayed in figures 2 and 3, where the RMS deviations for electron and ion temperatures and density are shown. The figure 2 includes 10 shots from the first group. Figure 3 includes shots from both groups with plasma current I_p > 1.5 MA.

The peaking of the electron temperature profiles (the ratio $T_e(0)/T_e(0.5)$) for shots with I_p>1.4 MA is shown in figure 4. It seen that most of points are in the narrow band $1.3 < T_e(0)/T_e(0.5) < 1.6$, and the peaking weakly decreases with increasing current. This means that the electron temperature profiles are approximately similar, and justifies our choice of the parameter $\mu_0=1/q_0$ in the canonical profile problem: $\mu_0 = (3.5 – 4)/q_a = (3.5 – 4)\ \mu_a$.

The electron-ion energy exchange power is high in the vicinity of the ETB due to low electron temperature. Therefore, the electron and ion temperature pedestals, $T_{e,ped}$ and $T_{i,ped}$, are close to each other, and so for simplicity, we sometimes use $T_{ped} = (T_{e,ped} + T_{i,ped})/2$ as the temperature pedestal. Figure 5 shows the calculated values of the temperature pedestal T_{ped}

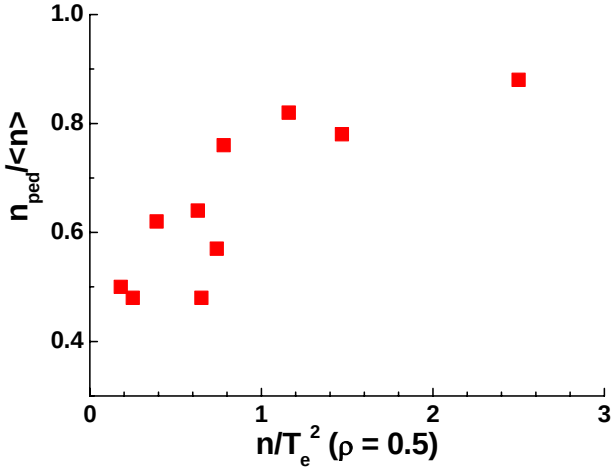

FIG. 7. Calculated normalized density pedestal for shots with I_p>1.5 MA.

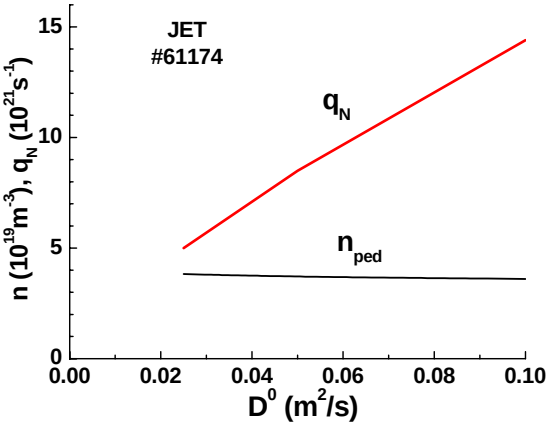

FIG. 8. Pedestal density n_{ped} and cold neutrals influx q_N. as functions of particle diffusivity.

versus plasma current. The main tendency is clear: the values of T_{ped} increase with current rise. It is may be explained by the decrease of temperature profile stiffness al low q_{cyl} (see Eq.(3)). Such behaviour of T_{ped} is observed usually in experiment.

In recent works [13-15], the peaking of the experimental density profiles in JET and ASDEX-U was considered. It was shown that in H-mode shots the peaking (the ratio $n(0)/<n>$) diminishes with increasing collisionality. Figure 6 shows the experimental and calculated density peaking factor versus collisionality for 10 JET shots with high current I_p > 1.5 MA. The experimentally observed trend of the peaking factor increasing with decreasing collisionality is well reflected in the calculated results. It is defined in the model by the increase of the anomalous particle pinch as the collisionality diminishes.

The rise of calculated normalized density pedestal with collisionality for shots with plasma current I_p > 1.4 MA is shown in figure 7. We see that a flattening of the density profile with increasing n/T_e^2, owing to the increasing importance of the density pedestal.

To estimate the reliability of the modelled density pedestal values, we temporarily relax constraint (6) and allow D^0 to vary in some range as a free parameter. Figure 8 shows the dependences of n_{ped} and q_N on D^0 with other parameters taken from shot #61174. Expression (6) gives us D^0 = 0.05. We see that the cold neutrals influx is proportional to D^0, but the density pedestal is really unchanged! This means that the density pedestal weakly depends on the transport barrier model, and that the modelled value of n_{ped} is robust. The physical explanation is that most of the cold neutral influx (up to 90%) is absorbed inside the ETB.

The comparison of the experimental, calculated and canonical relative gradients of pressure is shown in figure 9. The shown experimental values are averaged over time intervals Δt ranging from 0.6 – 2 s. The calculated values of R/L_p are very close to the experimental ones.

4. Modelling of ELM-free H-mode JET shots #41071 and #42623

These shots relate to the experimental campaign of 1997 with record fusion performance, but without tritium. They have the following features: (1) they are quite non-stationary; (2) during the ELM-free phase, which lasts 1.5 – 2.5 s, the plasma current decreases by 10%, and the plasma density rises from $<n> = 2\times10^{19}$ to 5×10^{19} m^{-3} (figure 10). The modelled time interval

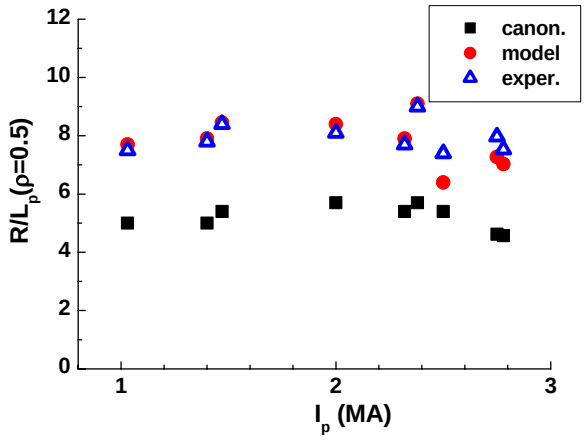

FIG. 9. Experimental, calculated and canonical relative gradients at $\rho = 0.5$.

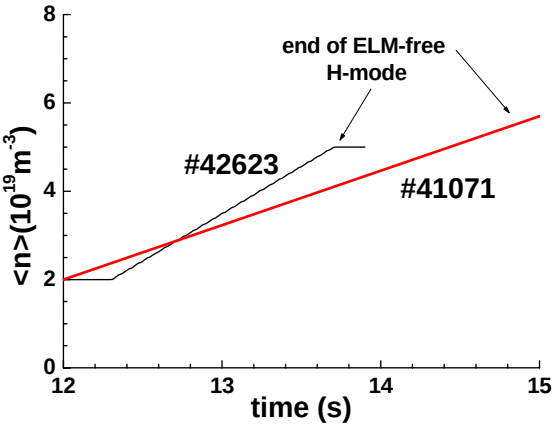

FIG. 10. Temporal evolution of density for JET ELM-free H-mode shots.

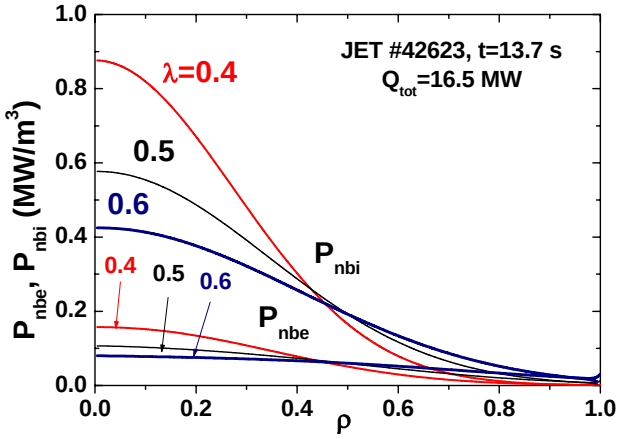

FIG. 11. Profiles of NBI power deposited to ions P_{nbi} and electrons P_{nbe} at different values of parameter λ.

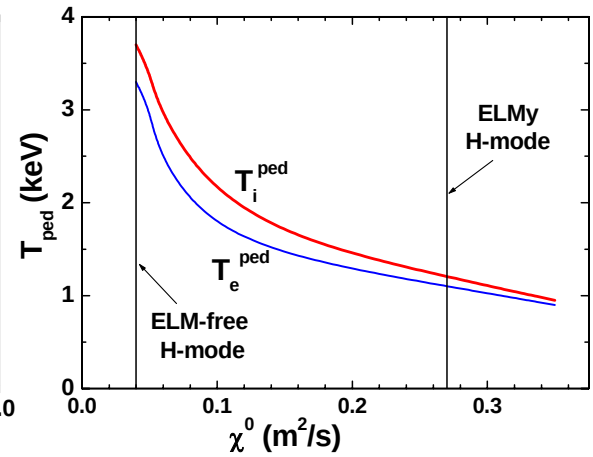

FIG. 12. Dependencies of the electron and ion temperature pedestals on the heat diffusivitiy for JET shots.

was 12s < t < 13.7 s for shot #42623, and 12s < t < 14.7 s for shot #41071. The NBI heating was switched on at t = 12 s and at the end of these time intervals there were giant ELMs (and so the calculations were stopped).

For the comparison of calculations with experiment we use in this section the "raw" experimental data for electron and ion temperatures and plasma density (and not data that were analyzed by TRANSP). To make clear the sensitivity of our calculations to the deposited power profiles, we use the following model. We fix the loss of hot particles to be 20%: Q_{abs} = 0.8 Q_{dep}, and assume that the fast ion density has a Gaussian radial profile $n_{hot} = n_{0,hot} \exp(-\rho^2/2\lambda^2)$. Here Q_{abs} and Q_{dep} are the absorbed and deposited powers, λ is a parameter equal to a half width of the fast ion density profile. Comparing with calculations by TRANSP for ELMy shots in the previous section confirms that our choice of multiplier 0.8 in Q_{abs} is reasonable for shots with $\langle n \rangle = (3 - 5)\times10^{19}$ m^{-3}, and suggests that λ lies in the range 0.4 – 0.6. The power densities, P_{nbe}, P_{nbi}, going from fast ions to the plasma electrons and ions were calculated using analytical expressions [16] and shown in figure 11 for shot #42623. It is seen that in the plasma centre the local values of P_{nbi} at λ = 0.4 and 0.6 differ by a factor of 2. In the ELM-free discharges, the pedestals are quasi-steady-state and their absolute values exceed the time-averaged values of pedestals in the ELMy discharges by a factor of 3-4.

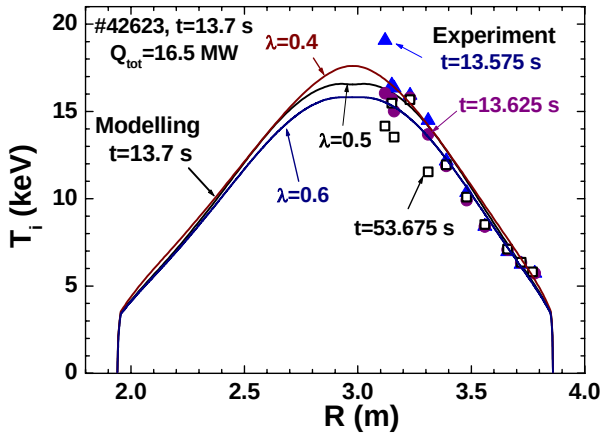

FIG. 13. The comparison of experimental ion temperature profiles from shot#42623 with calculated at different λ.

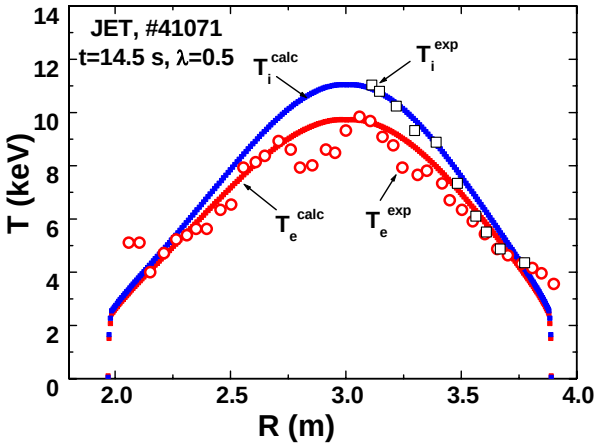

FIG.14. The comparison of experimental ion and electron temperature profiles from shot #41071 with calculated at λ=0.5.

These calculations have shown that to describe the temperature pedestals in the ELM-free discharges we have to diminish the heat diffusivities χ_e^0 and χ_i^0 by factor of 8-10 in comparison with (5, 6). This large factor arises due to the high stiffness of the temperature profiles. Figure 12 illustrates the dependence of the electron and ion temperature pedestals on the χ_e^0 and χ_i^0 for the shot #42623. Below in our calculations we reduce the constant multiplier 0.23 in (5) by a factor of 8-10 using the experimental estimates of the pedestal temperatures.

Calculated and experimental ion temperature profiles for shot #42623 are compared in figure 13. The experimental points are taken for three adjacent times spanning 75 ms. This allows one to estimate the scatter of experimental points. The calculated curves are drawn for λ = 0.4, 0.5 and 0.6. It is seen that all calculated curves reasonably describe the experiment. This feature arises again due to the stiffness of the temperature profile. The experimental and calculated profiles of ion and electron temperatures for shot #41071 (with λ = 0.5) are shown in figure 14. We see again the good accordance between experiment and model calculations.

The experimental and calculated plasma density profiles for shot #41071 at t = 14.5s are shown in figure 15. Note that these profiles are very flat. This feature is connected with a very fast density ramp. The anomalous particle pinch in the model is too weak to peak up the density profile by moving particles from the edge to the plasma centre. Apparently it is happened also in the experiment because of closeness of calculated and experimental profiles. Additional calculations have shown that a transition to a steady state scenario with saturated density leads to a density profile with higher peaking factor $n(0)/\langle n\rangle \sim 1.3 - 1.4$, which is close to the results shown in figure 6. Nevertheless, the steady state pressure profile in the model is close to profile in the transient scenario. The peaking of density does not change the peaking of pressure. This feature has to be verified in future experiments.

The effective heat diffusivities defined by the formula $\chi_{e,i}^{eff} = -q_{e,i}/(n\, dT_{e,i}/d\rho)$ are shown in figure 16. In the shot #42623 the deposited power is approximately two times larger than in shot #41071, so that the heat diffusivity coefficients rise by approximately a factor $2^{1/2} \sim 1.4$. In the gradient zone $\chi_{e,i}^{eff} \sim$ 2-3 m^2/s, but inside the transport barrier these coefficients are lower by approximately a factor of 100. The transport barrier width is approximately 3-4% of the minor plasma radius.

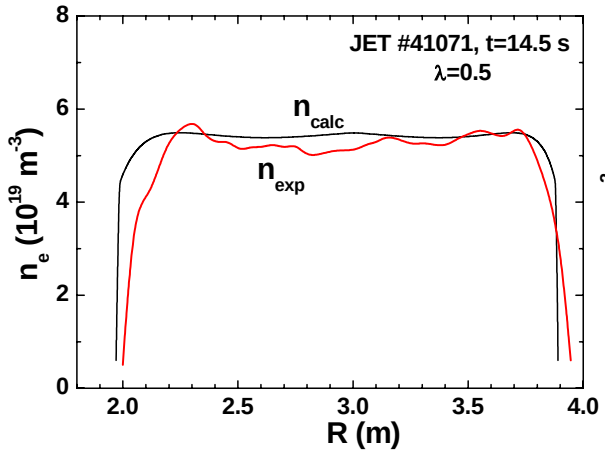

FIG. 15. The experimental and calculated plasma density profiles.

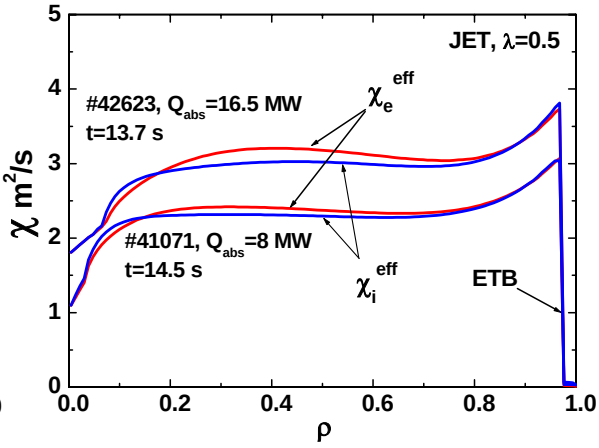

FIG. 16. The profiles of effective heat diffusiviy.

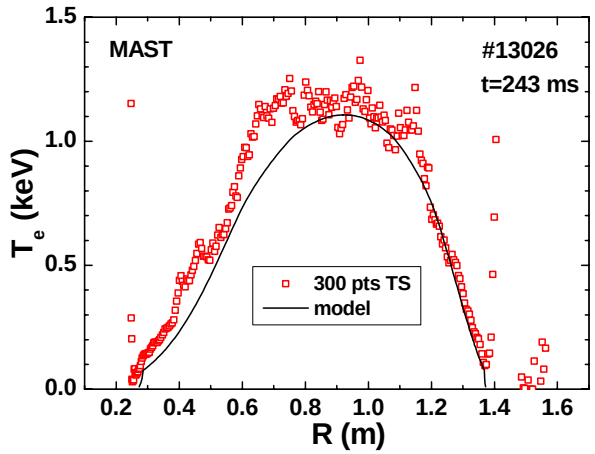

FIG. 17. The experimental and calculated electron temperature profiles in MAST.

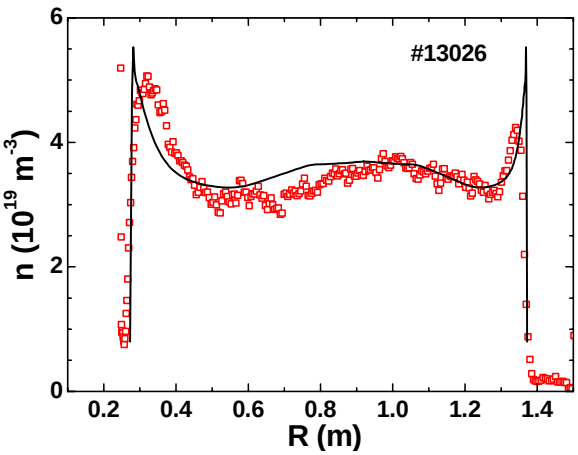

FIG. 18. The experimental and calculated plasma density profiles in MAST.

5. Simulation of MAST H-mode shots

MAST shot #13026 (I_p=0.75 MA, B_0=0.52 T, $\bar{n}$=3.5×10^{19} m^{-3}, P_{NB} =1.8 MW) was chosen for modelling. This shot demonstrates a rather long ELM-free phase just before the time of the Thomson scattering (TS) measurement. The simulated electron temperature and plasma density profiles are presented in figures 17, 18 and compared with data from the 300 point (opened squares) and 20 point (triangles) TS systems. Low value of B_0 leads to high temperature profile stiffness (see Eq. (3)), and, as a consequence, to low values of temperature pedestal both in ELMy and ELM-free shots. Therefore the same expressions (5, 6) were used for MAST also. We see that the simulations reproduce the peaked temperature profile and "ears" in the density profile.

6. Conclusion

The non-linear version of the CPTM has been applied to the modelling of JET and MAST ELMy and ELM-free H-mode shots. This version describes both the plasma core and the external transport barrier. It uses boundary conditions at the last closed magnetic surface and includes the possibility of bifurcations in the transport equations. Simulations have modelled the temperature and density pedestals reasonably well, and reproduce the main features of temperature and density profiles in H-mode shots. The electron temperature profiles have

been found to be similar over a wide range of plasma currents in JET. This leads to similarity in current density profiles that is in contrast with the L-mode shots. The model describes also the sharp dependence of the temperature pedestal on plasma current. This dependence was observed earlier in many tokamaks. The model allows one to describe also the increasing density profile peaking with decreasing collisionality, as was marked before in several experiments. The key features of the MAST density profiles are also reproduced.

Acknowledgments

The work is partly funded by the United Kingdom Engineering and Physical Sciences Research Council and by the European Communities under the contract of Association between EURATOM and UKAEA. The views and opinions expressed herein do not necessarily reflect those of the European Commission. This work was partly carried out within the framework of the European Fusion Development Agreement.

References

[1] COPPI, B., Comments Plasma Phys. Control. Fusion **5** (1980) 261.
[2] ESIPTCHUK, Yu.V. and RAZUMOVA, K.A., Plasma Phys. Control. Fusion **28** (1986) 1253.
[3] DNESTROVSKIJ, Yu.N., et al., Nucl. Fusion **46** (2006) 953.
[4] DNESTROVSKIJ, Yu.N., et al., Plasma Phys. Control. Fusion, **49** (2007) 1477.
[5] DNESTROVSKIJ, Yu.N. and PEREVERZEV, G.V., Plasma Phys. Control. Fusion **30** (1988) 47.
[6] REBUT, P.H., LALLIA, P.P. and WATKINS, M.L., Plasma Phys. and Control. Nucl. Fusion Research (Proc. 12th Int. Conf., Nice, 1988) IAEA, Vienna (1989) **2** 191
[7] RYTER, F., et al., Plasma Phys. Control. Fusion **43** (2001) A323.
[8] DNESTROVSKIJ, Yu.N., et al., Plasma Phys. Rep. **28** (2002) 887.
[9] DNESTROVSKIJ, Yu.N., DNESTROVSKIJ, A.Yu. and LYSENKO, S.E., Plasma Phys. Rep. **31** (2005) 529.
[10] DNESTROVSKIJ, Yu.N., et al., Nucl. Fusion (1995) **35** 1047.
[11] VOITSEKHOVITCH, I., et al., Proc. 33rd EPS Conf. on Plasma Physics, (Roma, 2006) ECA, **30I** P-1.078, http://epsppd.epfl.ch/
[12] DNESTROVSKIJ, Y.N., et al., Proc. 34th EPS Conf. on Plasma Physics, (Warsaw, 2007) ECA, **31I** P-4.125, http://epsppd.epfl.ch/
[13] VALOVIC, M., et al., Plasma Phys. Control. Fusion **46** (2004) 1877.
[14] ANGIONI, C., et al., Nucl. Fusion **47** (2007) L1-4.
[15] MASLOV, M., et al., this Conference, Rep. EX/P5-20.
[16] DNESTROVSKIJ, Y.N. and KOSTOMAROV, D.P., Numerical Simulation of Plasmas, Springer, Berlin, 1986.